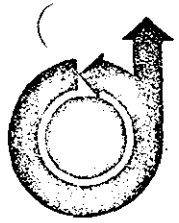

AIAA Paper
No. 70-726

TRACER MOLECULE SPECTROSCOPY APPLIED TO TURBULENT REACTIVE FLOWS

by
CLAYTON LaPOINTE and PHILIP C. MALTE
University of Michigan
Ann Arbor, Michigan

AIAA Reacting Turbulent Flows Conference

SAN DIEGO, CALIFORNIA/JUNE 17-18, 1970

-- NOTES --

TRACER MOLECULE SPECTROSCOPY APPLIED TO TURBULENT REACTI[illegible]LOWS*

Clayton LaPointe**
and
Philip C. Malte†

Gas Dynamics Laboratories
Department of Aerospace Engineering
The University of Michigan
Ann Arbor, Michigan

Abstract

The development of an experimental technique employing gaseous hydrogen fluoride as a tracer molecule, spectrally active in the infrared, to detect mixing rates and temperatures in turbulent and reacting flows is presented. Several initial investigations were undertaken. Subsonic air jets injected with hydrogen fluoride tracer were examined. Concentration profiles and mixing layer widths were obtained for cold, transonic, coaxially mixing jets of hydrogen with air and nitrogen with air. Ultimately the technique is to be applied to investigations of supersonic mixing and combustion. Supersonic combustion of hydrogen and air in a free coaxially mixing jet system has been obtained using a high pressure three phase arc heater to preheat the air. Preliminary temperature and mixing rate determinations using hydrogen fluoride spectroscopy and schlieren-photography are presented.

Nomenclature

a_ν	spectral absorptance
A	area
b	Lorentz half width
$B_\nu(T)$	Planck black body function
f(J, T)	state population factor
F	function defined by Eq. (11)
$g(\nu - \nu')$	monochromator slit function
I_ν	spectral radiance
J	rotational quantum number (lower state)
k_ν	absorption coefficient
K	equilibrium constant
ℓ	optical path coordinate
L	optical path length
m	molecular weight
M	Mach number
p	partial pressure
p_e	effective broadening pressure
r	radial coordinate
R_o	universal gas constant
R	jet radius
S	spectral line strength
T	temperature
w	mass flow rate
W	equivalent width of spectral line
x	non-homogeneous optical depth (Eq. (12))
y	perpendicular distance from jet centerline to optical path
α_s	broadening effectiveness of species
γ	ratio of specific heats
ρ	fluid density
ν	wavenumber
$\Delta\nu$	slit width

Subscripts

e	reference state
HF	hydrogen fluoride monomer
HFV	polymerized hydrogen fluoride vapor
m	spectral line center
o	reference state
t	total
TG	inner jet test gas

Superscripts

$(\bar{\ })$	measured quantity
o	incident

I. Introduction

The need for noninterfering diagnostic techniques to investigate flows with compressible

*Work performed under Contract F33615-67-C-1122, Air Force Aero Propulsion Laboratory, Wright Field, Ohio.

**Presently with the Scientific Research Staff, Ford Motor Company, Dearborn, Michigan.
†Graduate student, Department of Aerospace Engineering; presently on leave-of-absence from Martin Marietta Corporation, Denver, Colorado.

turbulent mixing and combustion is critical. Employment of immersed probes (chemical samplers, pitot tubes, thermocouples, hot wires) may be impossible, difficult or ambiguous in compressible and reacting flows. Flow field modification due to the probe's presence in supersonic flows is extensive. Chemical composition is altered by the probe's surface catalytic effect. As indicated by Cohen and Guile[1], the determination of high temperatures, such as those encountered in a hydrogen-oxygen flame, can be accomplished only by optical means. Spectroscopy offers an important method of determining chemical composition and thermodynamic state of a flow system in a noninterfering manner.

The modification of fluctuation fields by physical probes is also a serious consideration in some situations. For example, consider the enhancement of turbulent mixing in flows with combustion. Eschenroeder[2] has shown that turbulence is intensified by chemical heat release and Eschenroeder and Chen[3] have subsequently shown that eddy diffusivity is substantially increased. Their results depend on the phase relation between density fluctuations and chemical heat release (also expressible as a phase lag between density and pressure fluctuations) and in final form depend directly on $(\rho'/\bar{\rho})^2$. The concept of pressure-density phase coupling has been extended to the hydrogen-oxygen reaction in a mixing layer by Malte[4]. It appears that the correlation between density and pressure fluctuations may be a controlling factor in the chemical intensification of turbulence. Recent experimental studies by Glass[5] demonstrated the controlling effect of acoustic feedback on the spreading rate of underexpanded jets.

A noninterfering infrared spectroscopic technique using hydrogen fluoride as a tracer molecule has been designed, built, and tested at The University of Michigan Gas Dynamics Laboratories. The technique is well-suited for application to fuel-air mixing situations. With measurements of absorption and emission of radiant energy from a free mixing jet system it is possible to determine the temperature and spatial extent of the fluid which has been tagged with the spectrally active hydrogen fluoride tracer.

Hydrogen fluoride was chosen as the tracer gas for a number of reasons. It is a strong absorber in its fundamental vibration-rotation band centered at 2.5μ. The R-branch (Fig. 1) of this band extends into spectral regions devoid of atmospheric interference by CO_2 and H_2O, which are also common combustion products. The spectral line spacing is such that a single line may be easily isolated with monochromators of moderate resolution. Spectral line strengths and widths are known. Finally, its strong chemical bond allows its use at high temperature.

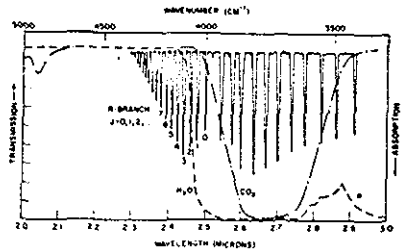

Fig. 1. HF Fundamental Vibration-Rotation Absorption Band (R and P Branches). Spectral Location of Water and Carbon Dioxide Absorption Bands Indicated.

This report, which is a summary of Ref. 6 and 7, presents a description of the experimental technique and results of investigations wherein hydrogen fluoride infrared absorption spectroscopy was used to obtain concentration profiles and temperatures in free submerged air jets injected with *hydrogen fluoride tracer.* Also, free, coaxially mixing streams of hydrogen and nitrogen with air have been examined. The data have been obtained in the subsonic and transonic regimes. Furthermore, supersonic combustion of a submerged jet has been obtained employing central injection of fuel (H_2) along with the hydrogen fluoride tracer into the arc heated air. These tests indicate that absorption and emission hydrogen fluoride spectroscopy can be utilized to obtain temperature and density in *reacting supersonic flows. Ignition* and reaction times can then be inferred.

II. Mathematical Formulation

Consider a cylindrically symmetric, nonhomogeneous medium upon which radiation, I_ν^o, is *directed as shown in Fig. 2.* The medium is characterized by phenomenological emission and absorption coefficients which are related to molecular and thermodynamic properties of its constituents. The spectral radiance emerging from the boundary nearest the observer is then given by the radiative transfer equation[8]

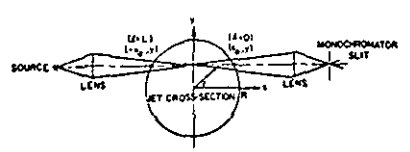

Fig. 2. Spectroscopic Coordinate System.

$$I_\nu(y) = I_\nu^o e^{-\int_0^L pk_\nu \, d\ell} + \int_0^L pk_\nu B_\nu e^{-\int_0^\ell pk_\nu \, d\ell} \, d\ell \qquad (1)$$

In this formulation, the condition of local thermodynamic equilibrium has been imposed by the use of Kirchhoff's law relating the emission and absorption coefficients to the Planck function, B_ν.

Pure Absorption

For gases at low temperatures, B_ν is small and the net relative loss of energy experienced by the incident beam is simply

$$a_\nu(y) \equiv \frac{I_\nu^o - I_\nu(y)}{I_\nu^o} = 1 - e^{-\int_0^L pk_\nu \, d\ell} \qquad (2)$$

In most infrared applications, the detecting instrument does not possess sufficient resolution to measure an undistorted line contour. The measured absorptance, $\overline{a_\nu}$, is related to the actual absorptance by means of the monochromator's slit function, $g(\nu - \nu')$.

$$\overline{a_\nu} = \frac{1}{\Delta\nu}\int g(\nu - \nu')\, a_{\nu'}\, d\nu' \qquad (3)$$

Here, the slit function is defined such that $g(0) = 1$ and $\int g(\nu - \nu')\, d\nu = \Delta\nu$, the spectral slit width. If the spectral line width, b, is much smaller than $\Delta\nu$, then $a_{\nu'}$ acts like a delta function situated at the line position, ν_m. Thus, for an isolated line,

$$\overline{a_\nu}\,\Delta\nu = g(\nu - \nu_m)\int a_{\nu'}\, d\nu' \qquad (4)$$

from which it follows that

$$\overline{W} \equiv \int \overline{a_\nu}\, d\nu = \int a_{\nu'}\, d\nu' \equiv W \qquad (5)$$

That is, the area encompassed by the measured absorptance profile equals the area under the actual absorptance profile. This area is termed the equivalent width of the line. Monochromators with equal sized exit and entrance slits, $g(\nu - \nu_m)$ is very nearly a triangle. Thus W may be obtained from a measurement of the peak absorptance, $\overline{a_{\nu_m}}$, and a calibration of $\Delta\nu$ versus mechanical slit width, i.e. $W = \overline{a_{\nu_m}}\,\Delta\nu$.

To relate $\overline{W}$ to the thermodynamic and molecular conditions at a point along the submerged optical path, the actual line profile, k_ν, and the mechanisms of line broadening must be taken into account. At moderate pressures and temperatures and in the infrared portion of the spectrum, collision broadening is the major broadening mechanism. It is described by the Lorentz dispersion contour[9],

$$k_\nu = \frac{S}{\pi}\frac{b}{b^2 + (\nu - \nu_m)^2} \qquad (6)$$

where

$$S = \int k_\nu \, d\nu \qquad (7)$$

is the line strength.

Combining Eq. (2), (5), and (6) and performing the integration assuming a homogeneous isothermal path leads to the familiar Ladenburg-Reiche[10] curve of growth,

$$W = 2\pi b x\, e^{-x}\left[J_o(ix) - iJ_1(ix)\right] \qquad (8)$$

for which there are the linear (weak line) and square root (strong line) approximations:

$$W \approx pSL \qquad (x \ll 1) \qquad (9)$$

and

$$W \approx 2\sqrt{bpSL} \qquad (x \gg 1) \qquad (10)$$

respectively. In the above $x = pSL/2\pi b$ and J_o, J_1 are Bessel functions of the first and second order. The awkwardness of Eq. (8) has lead to a number of simplified analytic approximations[11] to it even in this homogeneous case. The complete integration of the corresponding non-homogeneous equations to obtain a generalized curve of growth is not possible if $b = b(x)$. Simmons[12] has suggested the following approximation for the non-homogeneous, non-isothermal Lorentz contour.

$$k_\nu = \frac{S(x)}{\pi} F \frac{b_e}{b_e^2 + (\nu - \nu_m)^2} \qquad (11)$$

where F is a function which accounts for the variation of b(x) in the Lorentz contour: $F = b(x)/b_e$ in the strong line limit and $F = 1$ in the weak line limit. Here, b_e is the Lorentz half-width at some reference state. With this assumed contour, an approximate non-homogeneous Ladenburg-Reiche (modified L-R) curve of growth is obtainable and is

identical to Eq. (11) with b replaced by b_e and x replaced by

$$x_L = \frac{1}{2\pi b_e}\int_0^L pSF\,d\ell \qquad (12)$$

The weak and the strong line approximations may be readily extended to the non-homogeneous case without restricting the b variation.

$$W = \int_0^L pSd\ell \qquad (x_L \ll 1) \qquad (13)$$

$$\frac{W^2}{4} = \int_0^L bpSd\ell \qquad (x_L \gg 1) \qquad (14)$$

Note that the weak line approximation is independent of line width. If the line width is assumed constant along the path, the exponential in Eq. (2) may be expanded in series, the order of integration reversed in Eq. (5) and the resulting expression for W integrated term by term[7]. The result, to first order, is a nearly-weak curve of growth for constant b.

$$\int_0^L pSd\ell = \frac{W}{1 - \frac{0.078}{b_e}W} \qquad (0 < x_L \lesssim 1.5) \qquad (15)$$

In Fig. 3, the weak, nearly-weak and strong line approximations are compared to the Ladenburg-Reiche curve of growth. The weak and strong line approximations may be applied directly to the determination of density and temperature in their respective regions of applicability. The nearly-weak and the modified L-R form require some prior estimate of b_e. In practice, b_e was evaluated at the calculated centerline conditions.

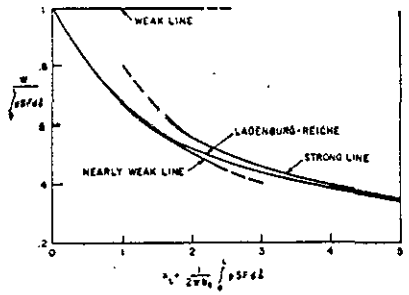

Fig. 3. Comparison of Line Growth Approximations.

Radial Profiles

We wish to infer radial temperature and density distributions from the radial profiles of the spectroscopic quantities which give rise to the measured path-integrated equivalent width. To do so, one must first perform an Abel transformation[13] of the transverse variation of W. Symbolically, we have the following correspondences:

Mode of Growth	Input		Transform
Weak	W(y)	=	p(r)S(r)
Nearly-weak	$\frac{W(y)}{1 - \frac{0.078}{b_e}W(y)}$	=	p(r)S(r)
Strong	$\frac{W^2(y)}{4}$	=	b(r)p(r)S(r)
Modified L-R	$W(y) - \frac{1}{2\pi b_e}\int_0^{L(y)} pSFd\ell = \frac{1}{2\pi b_e}p(r)S(r)F(r)$		

The latter case requires the use of a plot of the L-R function (Eq. (8)) to obtain

$$\frac{1}{2\pi b_e}\int_0^{L(y)} psFd\ell$$

from the measured W(y).

Inspection of the table shows that there are a *number of ways to interpret the transformed data* depending on the mode of line growth. If b_e is accurately known, the modified L-R curve of growth can generally be used to determine the mode. It is usually the case, however, that $b \ll \Delta\nu$ and therefore the line must be strongly absorbed to be detected at all. In that case, the measurement is of the product, b(r)p(r)S(r). The radial variation of this product is due to the variation of temperature, density (partial pressure) of the absorbing species and to some extent the density of species colliding with the absorbing species. Several independent measurements must therefore be made in order to solve for each unknown: p(r), $p_e(r)$, and T(r). This may be accomplished by measuring W(y) for several individual spectral lines. There may also be conditions under which the radial variation of bpS is due mainly to the variation of one parameter, such as p(r), and a considerable simplification in data interpretation results.

In the data reduction process, the Abel inversion technique of Nestor and Olsen[14] was programmed for digital computation. Where only centerline values are needed, a graphical technique[6] may be employed with good accuracy.

The following section describes the temperature and pressure dependence of S and b for collision broadened rotation-vibration lines arising from hydrogen fluoride absorption.

Line Strength and Lorentz Line Width

The computation of a diatomic molecule's rotation-vibration line strength in terms of molecular properties involves the solution of the quantum mechanical wave equation employing an appropriate internuclear potential. Once the wave functions are obtained, they, along with an experimentally determined dipole moment expansion, are used to form the dipole moment matrix. The dipole moment matrix is, in turn, related to the line strength by means of the Einstein transition probabilities, or alternatively, the oscillator strength. These operations are outlined by Penner[9] for general diatomic transitions. They have been performed, for the HF molecule, by *Meredith and Kent*[15] *who employed the HF data of* Lovell and Herget[16] and two assumed molecular models: the anharmonic oscillator and the Morse oscillator. The line strengths are calculated for temperatures between 273°K and 5000°K for several vibrational bands including the fundamental. These calculations have been extended to lower temperatures for the R branch of the hydrogen fluoride fundamental vibration-rotation band assuming no phase change (dilute gas)[6]. The variation of line strength with temperature is shown in Fig. 4.

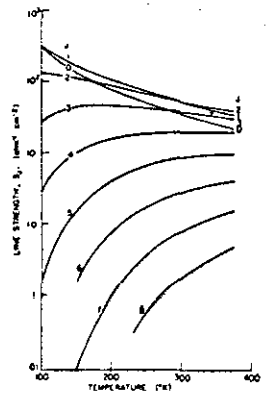

Fig. 4. Hydrogen Fluoride Line Strength versus Temperature; Fundamental Vibration-Rotation Band, R-Branch Rotational Quantum Number a Parameter.

The classical billiard ball collision model leads to the following expression for self-broadened Lorentz line width[8].

$$b = b_o \frac{p}{p_o}\sqrt{\frac{T_o}{T}} \qquad (16)$$

where the subscript signifies a reference state. A better approximation at low temperature is the resonant dipole-billiard ball (RDBB) collision model of Benedict, et al[17]. Simmons[18] has applied the RDBB model to the HF molecule and obtains an empirical expression for the Lorentz line width for multi-specie broadening:

$$b = b_o \frac{p_e}{p_o}\sqrt{\frac{T_o}{T}}f(J,T) \qquad (17)$$

where

$$p_e = \sum_s \alpha_s p_s \quad , \quad \text{effective broadening pressure}$$

α_s = broadening effectiveness of species, s

and f(J, T) is a state population factor. The temperature dependence of b/p_e for HF fundamental R-branch transitions is shown in Fig. 5.

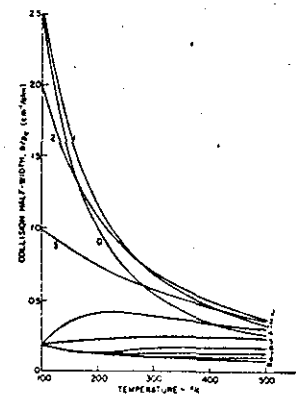

Fig. 5. Collision Broadened Spectral Line Half-Width for HF Molecules in the RDBB Approximation; Rotational Quantum Number (R-branch) a Parameter.

Since bpS, for a particular line, is quadratic in p in the self-broadened case, the line ratio technique may be used to determine, T(r). For this purpose, plots (Fig. 6) of b(J)S(J)/b(J')S(J') as a function of T may be constructed from

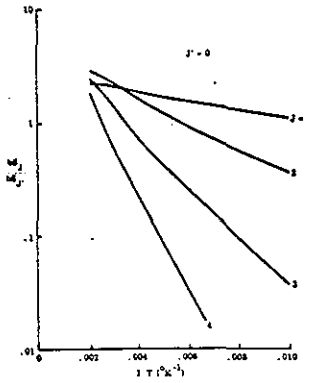

Fig. 6. HF Line Width-Strength Ratios, R-Branch Rotational Quantum Number a Parameter.

Fig. 4 and 5. Here J and J' refer to two lines characterized by their lower state rotational quantum numbers. Knowing T, the HF partial pressure may then be determined from

$$p^2 = \frac{(bpS) \text{ measured}}{\frac{b}{p}(T)S(T)} \qquad (18)$$

Pure Emission

In hot reacting flows, induced and spontaneous emission will occur. The emissive quantity which is analogous to the quivalent width is the total line radiance, $\mathfrak{L} = \bar{I}_\nu \Delta\nu$. The mode of growth which is analogous to the weak line approximation is the so-called "thin gas" approximation. Although the instrument resolution may still be such at $\Delta\nu \gg b$, the radiance may still be detectable provided the gas is sufficiently hot, i.e. $B_\nu(T)$ is large. In this approximation, the radiative transfer equation leads to

$$I(y) = \int_0^{L(y)} pSB_\nu \, dl \qquad (19)$$

Abel transformation of this equation yields the radial variation of the product, pSB_ν and the line ratio technique may be used to solve for T(r) using the line strengths reported earlier. In order to determine p(r), an absolute instrument calibration is then required.

In the event that self-absorption is not negligible, more elaborate techniques involving measurements with and without incident radiation, I_ν^0, may be employed[8].

III. Experimental Apparatus

The experimental set-up consists of an infrared spectrometer mounted on a servo-operated spatial scanning platform. Exhausting vertically through a hole in the platform is a coaxial mixing jet. A hydrogen fluoride injection system supplies either pure HF or HF mixed with another gas to the center outlet of the coaxial mixing jet. The entire system is remotely controlled.

Spectrometer Installation

A schematic of the spectrometer installation and data gathering system is shown in Fig. 7. A tungsten light source is focussed by an f/12 mirror system onto the transverse median plane of the jet. The emerging radiation is collected by a similar, but antisymmetric, mirror system and brought to a focus, after filtering, on the entrance slit of a Perkin-Elmer 98G monochromator. The spectrally resolved radiation is detected by an uncooled PbS cell. In absorption experiments, the radiation is chopped (100 Hz) at the source. For emission measurements, the chopper is located at the monochromator's entrance slit. Translation of the optical platform is in the y-direction of Fig. 2. Axial scanning is accomplished manually by repositioning the platform between runs.

A PAR 120 lock-in amplifier synchronously detects the chopped radiation and displays it on both an x-y and an x-t recorder. The x-t recorder is used for wavelength scanning while the x-y recorder is used for spatial scanning. Also displayed is the total source radiance. To further reduce noise in supersonic combustion experiments employing the arc heater, the PbS cell signal is preamplified at the monochromator.

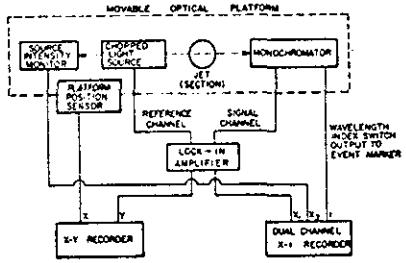

Fig. 7. Block Diagram of Optical Instrumentation.

Mixing Jets

Two coaxial mixing jet systems have been employed: cold subsonic and arc-heated supersonic. Both exhaust vertically into still air at atmospheric conditions. Figure 8 illustrates the subsonic mixing nozzle and flow field. The outer jet is room temperature air supplied by compressors. The inner jet is hydrogen fluoride, alone or premixed with either nitrogen or hydrogen. The mixing layer region is the region extending from the exit plane to the tip of the wedge-shaped potential annulus.

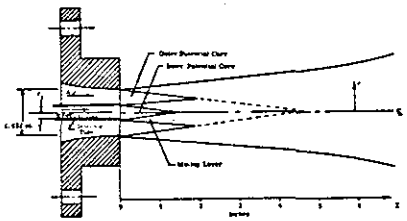

Fig. 8. Coaxial Free Jet Mixing Configuration for Absorption Experiments.

To apply the hydrogen fluoride tracer molecule technique to supersonic turbulent mixing with combustion, the previously described experimental setup, modified for emission spectroscopy, is utilized with a high pressure three phase AC arc heater system typically generating gas temperatures of 1500°K to 3000°K at pressures of 60 to 200 psig. A complete description of the arc heater and its performance is given by Geister[19]. The exit nozzle of the arc heater is of plug type. The supersonic plug nozzle, described in Ref. 7, features a water cooled centerbody where the fuel-hydrogen fluoride mixture can be injected into the hot arc-heated supersonic air stream. Expansion of the arc heated air to ambient pressure is primarily accomplished by a Prandtl Meyer expansion.

HF Injection

Hydrogen fluoride is shipped in steel cylinders as a liquid under its own vapor pressure which is approximately one atmosphere at room temperature. In order to pump the HF gas, the cylinder is immersed in a temperature controlled water bath. An upper limit is imposed upon the pressure attainable by this means because a new cylinder will become liquid-full approximately 140°F. The vapor pressure associated with this temperature is 44 psia. Because of this low maximum driving pressure, care had to be taken to minimize the pressure drop throughout the injection piping. Monel pipe (0.302 in. I.D.) was used as much as possible. A small pressure drop orifice is used to measure HF flow rate[6]. Pressures and temperatures were measured by gold-plated diaphragm transducers and Inconel-clad thermocouples, respectively.

Premixing of the hydrogen fluoride and test gas occurs at an ejector located several feet upstream from the nozzle exit. The center jet of the ejector, which consists of test gas, is expanded to low pressure supersonic flow, so that it can mix with the low pressure gaseous hydrogen fluoride. This mixture travels through 3 ft of 3/8 in. thin walled tube before mixing with the air jets for the cold experiments, and through approximately 2 ft of .30 in. pipe for the combustion experiments to insure fully developed pipe flow at the nozzle exit. To utilize the tracer nature of hydrogen fluoride its partial pressure in the inner jet is kept below 5%. Heating tapes are wrapped around the separate HF and test gas lines to help prevent HF condensation.

For subsonic jets the nozzle exit pressure is equal to atmospheric pressure; the necessary flow parameters at the nozzle exit are calculable. By assuming that the hydrogen fluoride is a perfect gas and that it is mixed uniformly with the test gas, the molecular weight of the inner jet is

$$m = \frac{w}{\frac{w_{HFV}}{m_{HFV}} + \frac{w_{TG}}{m_{TG}}} \qquad (20)$$

The inner jet Mach number is determined from the following expression of conservation of mass assuming no heat transfer

$$(w_{HFV} + w_{TG})\left(\frac{w_{HFV}}{m_{HFV}} + \frac{w_{TG}}{m_{TG}}\right) = \frac{\gamma p_o^2 A^2}{R_o T_t} M^2 \left[1 + \frac{\gamma - 1}{2} M^2\right] \qquad (21)$$

where the area, A, is that of the inside of the 3/8 in. inner jet injector tube modified for the actual velocity profile. The temperature, density, and velocity of the inner jet are then easily determinable.

Knowledge of the vapor state of the hydrogen fluoride is important. It is reported by Simons[20] that hydrogen fluoride vapor is in a polymerized state; for thermodynamic purposes the HF monomer may be considered in equilibrium with

its hexomer, H_6F_6

$$6HF = H_6F_6$$

Simons results are based on vapor density measurements; the apparent molecular weight of the polymerized "perfect gas" can be determined from the equilibrium constant,

$$\log_{10} K = \frac{40,000}{4.579T} - 43.145 \qquad (22)$$

where the equilibrium constant, K, is related to monomer partial pressure, p_{HF}, by

$$Kp^5 = \frac{1 - \frac{p_{HF}}{p}}{\left[\frac{p_{HF}}{p}\right]^6} \qquad (23)$$

and $p = p_{HF} + p_{H_6F_6}$, the total vapor pressure. The temperature, T, is expressed in °K and the pressure and reaction rate constant are expressed in millimeters of mercury. The molecular weight of the vapor is determined using Eq. (22) and (23), with the assumption that the individual species HF and H_6F_6 are both perfect gases; i.e.

$$m_{HFV} = 20\left[6 - 5\frac{p_{HF}}{p}\right] \qquad (24)$$

The molecular weight of the monomer gas HF is 20.

The equilibrium HF monomer partial pressure is shown in Fig. 9 plotted versus vapor pressure for the range of present operating temperatures. For typical conditions of hydrogen fluoride vapor in the heated cylinder, i.e. T = 100°F and P = 25 psia, the fractional monomer partial pressure is 0.65 and the vapor molecular weight is 55. Once the hydrogen fluoride is mixed with the nitrogen or hydrogen gas, its partial pressure is reduced to a few percent. Thus, if residence times are sufficient, the hydrogen fluoride should exist mainly as monomer HF with a molecular weight of 20 at the nozzle exit.

Spectroscopic measurement of the HF monomer partial pressure in the potential cores of the hydrogen and nitrogen cold jets showed that the hydrogen fluoride was chemically frozen at its initial unmixed composition. Only in the wake formed from the tube boundary layer was the HF partial pressure somewhat higher—indicating chemical relaxation due to the longer residence times. However, the inclusion of the foreign gas did prevent the hydrogen fluoride from condensing at the low temperatures (below its atmospheric boiling point of 67°F) encountered in the flow. For combustion experiments the high temperatures should eliminate any uncertainty concerning the hydrogen fluoride vapor state—the hydrogen fluoride exists as a monomer. However, for

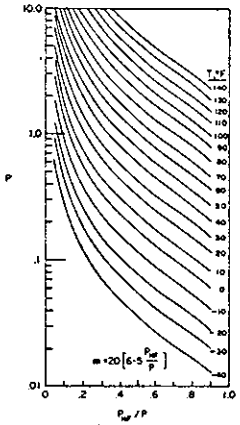

Fig. 9. Hydrogen Fluoride Equilibrium Vapor State.

further cold jet investigations it is planned to construct a heated stagnation chamber downstream of the ejector sufficient for relaxation of hydrogen fluoride to a monomer composition, before expansion and subsequent mixing.

IV. Experimental Results

HF-Air Subsonic Mixing Studies

To test the adequacy of the experimental method, absorption spectra were obtained with HF centrally injected into a cold subsonic air jet. Transverse equivalent width profiles of the first five R-branch lines were obtained at an axial position downstream of the potential region. The experimental conditions are summarized in Table 1. The

Table 1. Experimental Conditions

	HF	AIR	
Mass Flow Rate	1.04	92	gm/sec
Initial Jet Radius	0.159	1.46	cm
Stagnation Temperature	300	282	°K
Static Temperature	270	275	°K
Exit Mach Number	0.36	0.33	
Exit Velocity	1.4×10^4	1.1×10^4	cm/sec
Axial Location of Transverse Scan in Terms of Initial Radius	37	4	

untransformed transverse data is shown in Fig. 10.

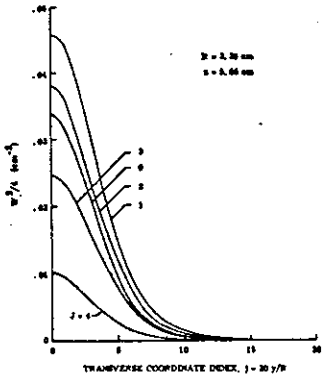

Fig. 10. Transverse Profiles of $W^2/4$.

Since the spectral resolution is such that only strongly absorbed lines are detectable, the appropriate Abel transformation program input is $W^2(y)/4$. The corresponding program output is bpS, the radial variation of the line strength-collision width product which, for small temperature variation, is proportional to p_{HF}^2. The square root of this quantity is normalized to its centerline value and shown in Fig. 11. The reason

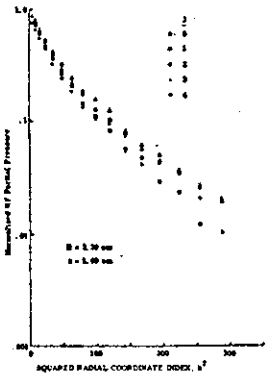

Fig. 11. Radial Variation of HF Partial Pressure Normalized to Centerline Value (k = 20r/R).

it is plotted on semi-log paper versus the radial index squared is to clearly indicate its gaussian behavior. Note that all curves exhibit gaussian radial depedence between the centerline and the point where bpS is approximately 20% of the centerline value. Beyond this point another gaussian, of different slope, could be fitted. This behavior is analogous to that reported by Becker et al[21] for the concentration field of smoke particles in a subsonic air jet. Indeed, these curves all reflect (some better than others) the radial variation of HF concentration. To see this, the temperature must first be obtained by the line ratio technique.

The ratio of the two most widely separated (J = 4, J' = 0) line strength-width products provides the most accurate temperature measurement. This ratio was obtained, point-by-point, as a function of radius and the curve of Fig. 6 used to determine T(r). The resulting temperature distribution is plotted in Fig. 12. Note the increasing scatter,

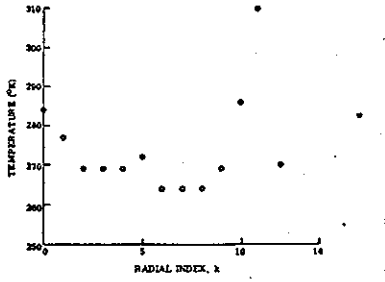

Fig. 12. Radial Variation of Temperature Calculated from J = 4, J' = 0 Strength-Width Product Ratio (k = 20r/R, R = 3.39 cm).

due to decreasingly accurate measurement of both numerator and denominator, as large radius is approached. Near the center of the jet, however, the temperature is constant at approximately 270°K. This temperature is, within a purely absorptive measurement's degree of accuracy, equal to the static temperature of the surrounding air jet. It indicates that the HF has come into thermal equilibrium with the much greater mass of air. It also indicates that temperature does not vary significantly, from an absorption point-of-view, in the radial direction. The entire variation of bpS is therefore due to the variation of HF number density or, equivalently, partial pressure.

Knowing temperature, one is now in a position to calculate N(r) and p(r) in the billiard-ball collision approximation. The curves of Fig. 11 may be formally identified with N(r)/N(0) or p(r)/p(0) provided the billiard-ball collision approximation is valid. The centerline values of N and p are compiled for the lines J = 1, 2, 3, 4 in Table 2.

Table 2. H .terline Number Density and Partial Pressure

J	N(0) (cm^{-3})	p(0) (atm)
1	1.81×10^{18}	.0650
2	1.87×10^{18}	.0678
3	1.79×10^{18}	.0649
4	1.81×10^{18}	.0656

Mixing Layer Studies: H_2, N_2, Air

In another series of experiments inner jets of nitrogen and hydrogen, premixed with tracer amounts of hydrogen fluoride, have been examined while coaxially mixing with an outer air jet. Attention was centered on the mixing layer between the inner and outer jet cores. The growth rate of mixing layers between parallel streams and in the initial regions of submerged jets is influenced not only by streamwise velocity differences and density levels but also by free stream turbulence and the wake formed from the initial boundary layers. Also, the effect of molecular weight may be important in the mixing and combustion of air with low molecular weight (H_2) fuel.

Nondimensional HF partial pressure profiles are presented in Fig. 13 and 14 for mixing layers between nitrogen and air jets; Fig. 15 and 16 show mixing between hydrogen and air jets. The Mach numbers of the nitrogen and hydrogen jets were varied from 0.3 to 0.9, while the outer air jet Mach number was varied from 0.3 to 1.1. The light beam was centered 3.78 injector radii downstream of the injector exit. The radius of the injector tube was 0.156 in. Experimentally obtained path-integrated absorptances were Abel inverted using the nearly-weak and the strong line approximation where applicable. The Lorentz half-width was estimated from temperature and flow rate measurements of the hydrogen fluoride and test gas. Ideally, number density ratio, HF monomer/test gas, should be constant across the mixing layer. The HF concentration profiles are assumed equal to corresponding profiles of the test gas with which the HF is premixed because the turbulent motions are assumed to make no distinction between gas type and molecular diffusion is negligible.

The concentration profiles all exhibit the same general shape; throughout most of the mixing layer the decrease in partial pressure is linear. As shown by Abramovich[22] one expects a linear decrease in concentration through subsonic mixing layers. Near the outer edge of the mixing layer a more gradual approach to the outer air conditions is noted. Concentration profiles obtained at like flow conditions were slightly higher for the J = 0 HF spectral line than for the J = 4 line. This is an effect probably resulting from minor data reduction or spectroscopic approximations.

The inner jet core is taken to extend from the jet system centerline to the point where the partial pressure profile begins to drop-off rapidly, indicating the start of the mixing layer. Some scatter is seen in the values of HF partial pressure measured in the core. The maximum value of HF partial pressure generally existed at the point which is

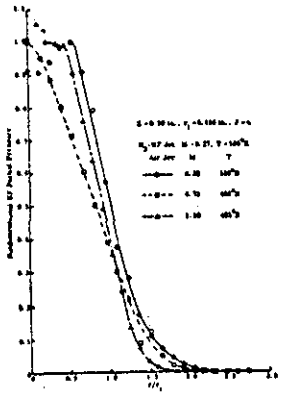

Fig. 13. Coaxial Mixing Between Inner N_2-HF Jet and Outer Air Jet.

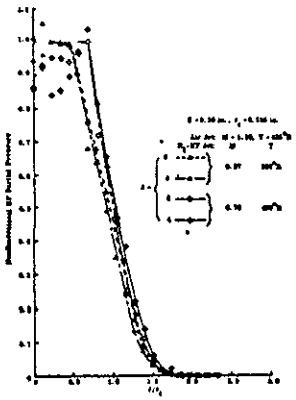

Fig. 14. Coaxial Mixing Between Inner N_2-HF Jet and Outer Air Jet.

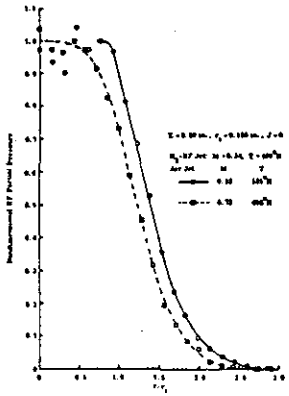

Fig. 15. Coaxial Mixing Between Inner H_2-HF Jet and Outer Air Jet.

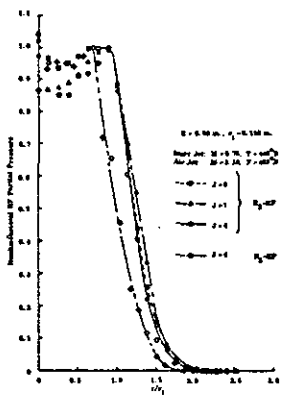

Fig. 16. Coaxial Mixing Between Inner H_2-HF Jet and Outer Air Jet.

taken to be the core edge. This value gave the best results for nondimensionalization of the profiles. The peak in the profiles, at the core edge, is probably due to increased HF monomer resulting from longer residence times in the boundary layer of inner jet.

Mixing layer widths are plotted versus nondimensional mass flux difference in Fig. 17. The data is taken from Fig. 13 to 16 as well as from additional experiments. In general, the results show increased mixing layer width for increased mass flux difference, and decreased mixing at increased Mach number. The mixing layer widths are taken to be the distance from the peak partial pressure to the point where the partial pressure is 2% of its peak value. The widths obtained are much larger than those predicted by mixing layer growth rate formulas. Thus, it appears that free stream turbulence and the wake formed from the initial boundary layers dominate the mixing. Only at large values of nondimensional velocity difference do the results approach values predicted using the growth rate expressions (corrected for density) given by Abramovich[22]. Furthermore, the mixing layer widths are fairly insensitive to gas type.

Since the selection of the "correct" mixing layer width is sensitive to the shape of the HF partial pressure profile in the vicinity of the inner and outer jet cores, the partial pressure half-radius, being more easily selected, was determined. The half-radius, defined as the point where p_{HF} is equal to one-half its peak value is plotted in Fig. 18 versus a mixing parameter that corrects the standard velocity difference formula

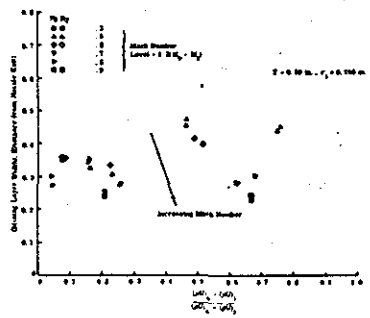

Fig. 17. Mixing Layer Widths Between Inner Jets of Nitrogen and Hydrogen Mixing with an Outer Air Jet.

for the difference in stream densities. A linear increase with mixing parameter is indicated. The half-radii of the hydrogen mixing layers are larger than those for the nitrogen jets. Thus, for similar mixing layer widths, the areal extent of mixed hydrogen and air is greater than that for mixing of nitrogen and air. For zero velocity difference, the mixing layer half-radii appear to originate from the radius of the inner jet injector tube—as intuitively expected. Half-radii for mixing layers of submerged N_2 and H_2 jets are also shown; the values are consistent with those of mixing layers between coflowing jets.

Supersonic Combustion

Supersonic combustion has been obtained using the high pressure three phase arc heater with plug nozzle. The arc-heated air forms the outer jet, while the centrally injected cold hydrogen fuel with hydrogen fluoride tracer forms the inner jet of the free-coaxial, turbulently mixing and reacting jet system. Schlieren photographs of reacting and nonreacting jets are shown in Fig. 19 and 20, respectively. A vertical knife-edge, parallel to the jet system centerline, was used to show density gradients in the transverse direction. For the reacting case the hydrogen flow rate was 0.002 lbm/sec while that of the air was 0.115 lbm/sec—slightly fuel lean. The arc chamber pressure was 195 psia and its calculated temperature was 1800 °K. The air jet had a Mach number of about 2.0 and appears to constrict the inner jet (most likely to sonic conditions). The nonreacting case used nitrogen at approximately the same driving pressure and at 0.007 lbm/sec, substituted for hydrogen. While the nondimensional mass flux difference between the initial streams is greater in the hydrogen case—indicating increased mixing—the amplified spreading rate of the composite submerged jet is felt to be mainly due to combustion and the effect of combustion on the mean flow (density, velocity, and flow direction) and the turbulent fluctuations. The reacting jet begins to spread more rapidly than the nonreacting jet at a distance of slightly more than two diameters downstream. This is interpreted as the start of significant combustion, and the corresponding time delay, for an average jet velocity of 4000 ft/sec, is 3×10^{-5} sec. The density difference between inner and outer jets is detectable at greater distances in the nonreacting case than in the reacting case; this also indicates increased cross-stream mixing in the reacting case. A large portion of the reacting jet—*essentially the region encompassed by the photo*graph of Fig. 19 appeared very luminous.

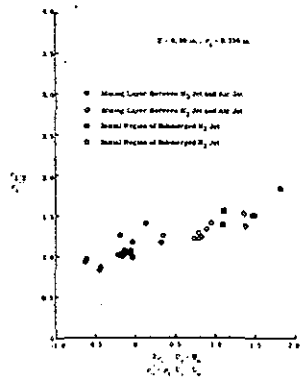

Fig. 18. Half Radius Based on Partial Pressure for N_2 and H_2 Jets Mixing with Coaxial Air Jets and Ambient Atmosphere.

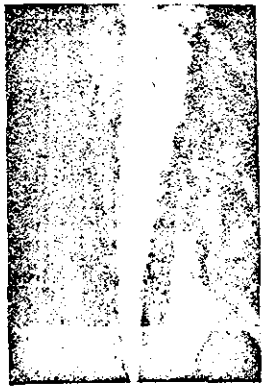

Fig. 19. Reacting Turbulent Supersonic Jet.

Preliminary spectroscopic measurements using hydrogen fluoride have been obtained for the above inner jet flow conditions but with slightly different hot air conditions, i.e. chamber temperature of 2000°K and pressure of 115 psia, flow rate of 0.065 lbm/sec and expanded Mach number of about 1.8. A trace of spectral output showing the J = 1 HF line at cold conditions, and a subsequent partial radial scan at combustion conditions is presented in Fig. 21. The optics were centered 2.38 in., i.e. 3 1/2 diameters, downstream from the nozzle exit; the black body temperature of the lamp at the wavelength corresponding to the J = 1 HF spectral line was 1150°K. Figure 18 indicates that, without combustion the average isothermal jet temperature is less than the black body source temperature (1150°K) and that, with combustion, it is greater than 1150°K.

Fig. 20. Nonreacting Turbulent Supersonic Jet.

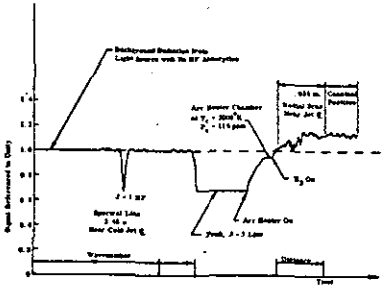

Fig. 21. Spectroscopic Output at 2.48μ During Supersonic Combustion.

Because the part of the HF spectrum examined is known to be isolated from regions of H_2O and CO_2 radiation, and since H_2, O_2, and N_2 are spectrally inactive, the measured emission is due to HF. Furthermore, a spectral scan of the spectrum with combustion showed distinct R branch HF lines still separated from water vapor lines. No evidence of combustion inhibition by the hydrogen fluoride was observed. *If reaction of HF with* any species present in the reacting gases occurred, or if the HF dissociated, the degree was insufficient to eliminate the spectrally active HF.

V. Conclusions

This study was undertaken to develop tracer molecule diagnostics using hydrogen fluoride for application to turbulently mixing and reacting flows. Mixing in cold, radiatively absorbing jets has been investigated; the tracer technique appears to be very useful when the vapor state of the hydrogen fluoride is chemically frozen. Hydrogen fluoride concentration profiles can then be equated to those of the fluid which has been tagged with tracer. By proper selection of the hydrogen fluoride spectral line, temperature, and flow rate precise concentration profiles and mixing rates are determinable. The technique is an important diagnostic aid in compressible flows where a physical probe would adversely affect the turbulent structure. Future investigations of radiatively absorbing cold jets will employ a heated stagnation chamber to insure a constant hydrogen fluoride monomer state.

Supersonic combustion in a submerged jet system has been obtained. The combustion caused a marked increase in the jet spreading rate when compared to a nonreacting "similar" jet system using inert nitrogen substituted for hydrogen. Preliminary investigations using the hydrogen fluoride tracer in reacting jets have been made; an emission of radiative energy was detected for the R branch HF spectral lines and these lines appeared stable at high temperature with no noticeable combustion inhibition by the HF. The technique will be utilized in a series of experiments employing turbulent mixing with combustion.

Acknowledgment

This work was performed under contract with *the Air Force Aero Propulsion Laboratory, Wright* Field, Ohio. The project was initiated and directed by Professor J. A. Nicholls of The University of Michigan's Gas Dynamics Laboratories.

References

1. Cohen, L.S. and Guile, R.N., "Investigation of the Mixing and Combustion of Turbulent, Compressible Free Jets," CR-1473, December 1969, NASA.

2. Eschenroeder, A.Q., "Intensification of Turbulence by Chemical Heat Release," Physics of Fluids, Vol. 7, November 1964.

3. *Eschenroeder, A.Q. and Chen, Tung,* "The Spectrum of Turbulence in an Exothermal Gas Flow," GM Defense Research Laboratories Report TR 63-217F, November 1963.

4. Malte, P.C., "Turbulent Transport in a Combusting Shear Flow," Paper No. 68-27, Fall Meeting of the Combustion Institute, *Western States Section, Menlo Park, California*, October 1968.

5. Glass, D.R., "The Effects of Acoustic Feedback on the Spread and Decay of Supersonic Jets," AIAA Paper No. 68-80, January 1968.

6. LaPointe, C.W., "An Experimental Study of Coaxial Turbulent Mixing of Liquid and Gaseous Fuel with Air," Air Force Aero Propulsion Laboratory Report AFAPL-TR-69-64, Wright-Patterson Air Force Base, August 1969.

7. Malte, P.C. and Nicholls, J.A., "Hydrogen Fluoride Tracer Molecule Spectroscopy Applied to Turbulent Mixing and Combustion," to be published as Air Force Aero Propulsion Laboratory Report, 1970.

8. Simmons, F.S., "Spectroscopic Pyrometry of Gases, Flames, and Plasmas," ISA Transactions, Vol. 2, No. 2, 1963.

9. Penner, S.S., Quantitative Molecular Spectroscopy and Gas Emissivities, Addison-Wesly, New York, 1959.

10. Ladenburg, R. and Reiche, F., "Uber Selektive Absorption," Am. Physik 42, 181, 1913.

11. Tien, C.L., "A Simple Approximate Formula for Radiation from a Line with Resonance Contours," JQSRT, 6, pp. 893-894, 1966.

12. Simmons, F.S., "Radiances and Equivalent Widths of Lorentz Lines for Non-Isothermal Paths," JQSRT, 7, 111-121, 1967.

13. Bracewell, R., The Fourier Transform and its Applications, McGraw-Hill, New York, 1965.

14. Nestor, O.H. and Olsen, N.H., "Numerical Methods for Reducing Line and Surface Probe Data," SIAM Rev., 2, 3, July 1960.

15. Meredith, R.E. and Kent, N.F., "Line Strength Calculations for the 0 → 1, 0 → 2, 0 → 3, and 1 → 2 Vibration-Rotation Bands of Hydrogen Fluoride," Willow Run Laboratories, Report 4613-125-T, The University of Michigan, April 1966.

16. Lovell, R.J. and Herget, W.F., "Lorentz Parameters and Vibration-Rotation Interaction Constants for the Fundamental Band of HF," J.O.S.A., 52, 1374-1376, 1962.

17. Benedict, W.S., Herman, R., Moore, G.E., and Silverman, S., "The Strengths, Widths, and Shapes of Infrared Lines, parts I and II," Can. J. Phys., 34, 830-875, 1956.

18. Simmons, F.S., "Infrared Spectroscopy Study of Hydrogen Fluoride Flames," Ph.D. Thesis, The University of Michigan, 1966.

19. Geister, D.E., "Characteristics of a High Pressure AC Arc Heater System," Aerospace Research Laboratories Report, No. 67-0217, Wright-Patterson Air Force Base, December, 1967.

20. Simons, J.H., Fluorine Chemistry, Vol. I, Academic Press Inc., 1950.

21. Becker, H.A., Hottel, H.C., and Williams, G.C., "The Nozzle-Fluid Concentration Field of the Round, Turbulent, Free Jet," J. Fluid Mech., 30, 2, 285-303, 1967.

22. Abramovich, G.N., The Theory of Turbulent Jets, M.I.T. Press, 1963.